Geophysical Research Letters

RESEARCH LETTER
10.1029/2018GL079363

Understanding Melting due to Ocean Eddy Heat Fluxes at the Edge of Sea-Ice Floes

Christopher Horvat[1,2] **and Eli Tziperman**[2]

[1]Institute at Brown for Environment and Society, Brown University, Providence, RI, USA, [2]Department of Earth and Planetary Sciences, Harvard University, Cambridge, MA, USA

Key Points:
- Submesoscale ocean eddies energized at static melting sea-ice edges may lead to heat transport between open ocean and ice-covered areas
- Such eddies may determine the melting rate of sea ice yet cannot be represented in current climate models
- We outline a representation of these eddy heat fluxes that captures the melting of sea ice that can be used to improve future sea-ice models

Supporting Information:
- Supporting Information S1

Correspondence to:
C. Horvat,
horvat@brown.edu

Citation:
Horvat, C., & Tziperman, E. (2018). Understanding melting due to ocean eddy heat fluxes at the edge of sea-ice floes, *Geophysical Research Letters*, *45*, 9721–9730. https://doi.org/10.1029/2018GL079363

Received 26 JUN 2018
Accepted 10 SEP 2018
Accepted article online 14 SEP 2018
Published online 27 SEP 2018

Abstract Understanding how upper-ocean heat content evolves and affects sea ice in the polar regions is necessary to predict past, present, and future weather and climate. Sea ice, a composite of individual floes, varies significantly on scales as small as meters. Lateral gradients in surface forcing across sea-ice concentration gradients can energize subgrid-scale ocean eddies that mix heat in the surface layer and control sea-ice melting. Here the development of baroclinic instability near floe edges is investigated using a high-resolution ocean circulation model, an idealization of a single grid cell of a climate model partially covered in thin, nearly static sea ice. From the resulting ocean circulation we characterize the strength of eddy-induced lateral mixing and heat transport, and the effects on sea-ice melting, as a function of state variables resolved in global climate models.

Plain Language Summary Sea ice is intrinsically tied to the ocean it forms out of, but the evolution of the Arctic ocean remains poorly understood thanks in part to the sea ice itself, which makes both travel and remote sensing extremely difficult. The increasing computing power available to climate modelers may be a poisoned chalice: Sea-ice models are built on a continuum framework and cannot therefore realize the sharp and heterogeneous concentration differences that may energize ocean circulation and thereby control sea-ice melting. We begin the process of incorporating these kind of effects in sea-ice models by describing and parameterizing the summertime response of the ocean to an idealized sharp sea-ice edge, providing guidance on how this methodology can be simplified and further implemented in continuum sea-ice models while maintaining the impacts of these coupled effects.

1. Introduction

Through its albedo and mediation of ocean-atmosphere heat exchange, Earth's sea-ice cover plays an important role in the climate system. Arctic sea-ice volume has declined rapidly in the satellite era, leading to a reduction in surface albedo that is the main cause of the rapid warming of the Arctic Screen and Simmonds (2010). The loss of Arctic sea ice coincides with a transition from a thick, perennial sea-ice cover to a seasonal one: Most of the current Arctic Ocean is covered in thin, first-year ice that grows in winter and melts entirely in summer (Kwok & Rothrock, 2009; Maslanik et al., 2011; Stroeve et al., 2012). The growth of sea ice in winter is tightly coupled to the depth and heat content of the ice-covered ocean mixed layer, major uncertain factors in the polar climate system (Peralta-Ferriz & Woodgate, 2015). Nearly half of the melting of summer Arctic sea ice occurs at its base, that is, due to heat fluxes from the ocean to the ice (Lei et al., 2014; Perovich, 2003). In turn, the seasonal cycle of ocean heat content is coupled to the seasonal evolution of sea ice, which mediates the heating and mixing of the polar oceans. This coupling has contributed to a lengthening of the Arctic sea-ice melt season over the satellite era as the Arctic Ocean has warmed and Arctic sea ice has retreated (Markus et al., 2009).

Sea ice is a composite of individual floes, each identified with a horizontal scale, or "size." Floe sizes span a wide range, and play a critical role in floes' thermodynamic evolution. For floes smaller than 100 m, lateral (along the floe edge) melting is a dominant component of thermodynamic evolution of sea ice (Horvat & Tziperman, 2015; Steele, 1992). Yet ocean eddies with scales of several kilometers or smaller may be energized in regions where gradients in sea-ice concentration lead to gradients in upper-ocean properties, such as within the marginal ice zone (e.g., Hakkinen, 1986; Manucharyan & Thompson, 2017) or at an ice edge (Årthun et al., 2013; Matsumura & Hasumi, 2008).

While there have been limited and indirect observations of the impact of kilometer-scale ocean variability at floe edges in summer (e.g., Perovich, 2003), eddies generated at floe boundaries during the melt season have the potential to mix ocean heat laterally from the warmer open water to under the ice. This eddy heat transport can melt sea ice at its base near floe edges, leading to a strong dependence of the melting rate of sea ice on floe size. This process is active for larger floes, where lateral melting is not a major factor and for which size-dependent melting is not applied in current climate models (Horvat et al., 2016). Current ocean/sea-ice models assume that any heating applied to open water by the atmosphere is instantaneously mixed throughout the grid cell, though in reality there is a partitioning of heat content between open water regions and under-ice regions (Holland, 2003). Unfortunately, current sea-ice models are coarse continuum models, and are still not capable of resolving ocean mixing across floe edges within a given ocean model grid cell. The mechanical interactions between sea ice, ocean eddies, and upper ocean density structure in the marginal ice zone have been explored by Manucharyan and Thompson (2017), but the understanding of thermodynamic and melting-induced feedbacks is still lacking.

The purpose of this work is to focus on the development of baroclinic instability near a floe edge during the melt season, and understand the effects of the developing eddies on sea-ice melting. We use a high-resolution ocean circulation model, representing an idealization of a single grid cell of a climate model partially covered in thin, static sea ice. The idealizations, including an ocean that is initially at rest and lack of wind forcing and therefore a nearly stationary sea ice, allow us to carefully study the thermodynamic ice-ocean coupling. We characterize the strength of eddy heat exchange and subsequent sea-ice melting using parameters accessible to coarser continuum climate models. This extends the study of Horvat et al. (2016), moving towards a parameterization of the effect of these ocean eddies for climate modeling purposes. We neglect dynamic effects related to ice movement, thus complementing the idealization of Manucharyan and Thompson (2017) who made the opposite assumption, neglecting thermodynamic feedbacks.

2. Methods

The Arctic is rapidly transitioning from a perennial sea-ice regime to a seasonal one, where the majority of Arctic sea ice is relatively flat first-year sea ice that melts during the summer season (Kwok & Rothrock, 2009; Stroeve et al., 2012). We therefore design ocean circulation model experiments that represent melting at the edge of, or near a newly opened gap in, first-year sea ice in summer, when the ice and ocean are exposed to strong shortwave radiative forcing. Model simulations use the MIT general circulation model (Losch et al., 2010; Marshall et al., 1997) and simulate sea-ice evolution based on the two-layer thermodynamic model of Winton (2000). Vertical mixing is realized using the K-profile parameterization (Large et al., 1994). The ice-ocean heat flux is computed using a bulk heat transfer parameterization appropriate for marginal ice zones (McPhee, 1992; McPhee & Morison, 2008).

There is no explicit horizontal diffusion of temperature and salinity. Horizontal eddy viscosity is represented by the Smagorinsky scheme. We use an adapted version of the Deremble et al. (2013) atmospheric boundary layer model to simulate the turbulent fluxes between the ocean, sea ice, and atmosphere, as discussed in Horvat et al. (2016). The ice is free to move, though there is no applied wind stress in our prescribed forcing fields and the initial ocean currents are set to zero. Dynamical ice effects are therefore weak compared to thermodynamic ones, which allows us to explore a purely thermodynamically driven regime.

The model domain is a rectangular, zonally re-entrant channel, 60 km by 30 km by 1,000 m. The horizontal grid spacing is 100 m, with a vertical grid spacing of 1 m over the top 50 m, increasing by 20% at each subsequent grid point. The ocean is initialized using July climatological temperature and salinity profiles from the Fram Strait at 80°N, 0°E (Carton & Giese, 2008), with the top 50 m of the water column homogenized to create a mixed layer. Initially the northern half of the model domain is covered by sea ice with a concentration of 100%, thickness of 1 m, and internal temperature of −5 °C. The top 50 m of the initial ocean temperature field is seeded with white noise uniformly distributed between ±0.025 °C. The atmospheric radiative forcing fields include a horizontally and temporally uniform (no diurnal cycle) shortwave forcing of 320 W/m^2 and a longwave forcing of 240 W/m^2, drawn from May–July climatological averages at 80°N, 0°E. The forcing leads to a net heating of roughly 100 W/m^2 in the open water and a net heating of 10 W/m^2 of the ice. We examine the sensitivity of the results that follow to the initial stratification, applied forcing, and ocean-ice exchange in Figures S1–S3 in the supporting information.

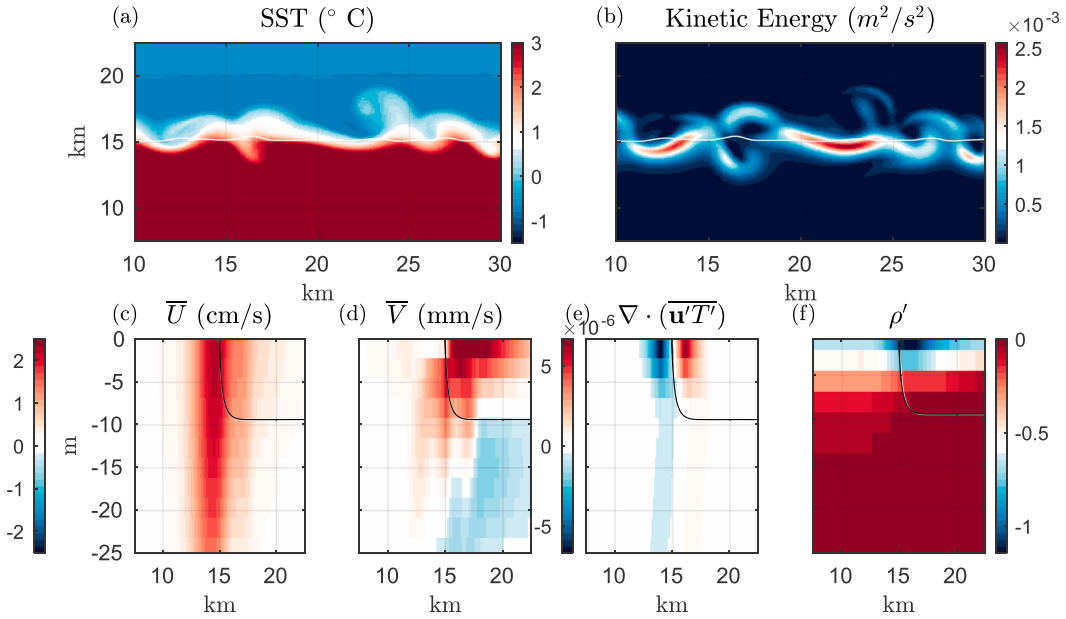

Figure 1. Ocean circulation in the ice-edge experiment. (a–f) Fields at day 14 of the simulation. (a) Top 10-m average ocean temperature. (b) Top 10-m average ocean kinetic energy. White line in (a)–(b) denotes the position of the ice edge. (c) Zonal average along-ice-edge velocity field $\overline{u}$ in units of cm/s. (d) Zonal average cross-ice-edge velocity field $\overline{v}$ in units of mm/s. Plots (c)–(d) share a single color bar. (e) Eddy temperature transport $\nabla \cdot \left(\overline{v'T'}, \overline{w'T'}\right)$. (f) Zonal mean density anomaly. Black line in (c)–(f) is zonally averaged sea-ice thickness curve, multiplied by −10, at day 14.

3. Results

Figures 1a–1f show the ocean circulation that develops at the ice edge by model day 14. The prescribed heat fluxes warm the ice-free region, and also lead to sea-ice melting (Figure 1a). Under-ice regions are then cooler and fresher than ice-free regions, and a buoyancy gradient develops at the surface near the ice edge (Figure 1f) that is dominated by the cross-edge salinity gradient. As the sea ice melts, the under-ice freshwater forcing strengthens the vertical stratification. Before an ocean circulation and mixing can develop, this surface lens of fresher water is confined to just below the sea-ice base. The cross-ice edge buoyancy gradient is balanced by an along-ice-edge jet with magnitude $\overline{u}^x$, where $\overline{(\cdot)}^x$ indicates a zonal mean along the ice edge (Figure 1c, units of cm/s). A comparatively weak ageostrophic secondary circulation of magnitude $\overline{v}^x$ develops perpendicular to the along-ice-edge jet (Figure 1d, units of mm/s). As the ocean circulation grows, vertical motions associated with the ageostrophic circulation and eddies mix the fresh top ocean model layer with the saltier water below, deepening the penetration of fresh water near the ice edge. Were the sea ice in greater motion, stress at the ice-ocean interface would lead to a shear in the under-ice velocity profile, and vertical mixing that could deepen the freshwater lens, and therefore weaken the horizontal density gradient and resulting along-edge jet, though this effect is weak in these experiments.

As the effect of temperature on density is small compared to that of salinity, the ageostrophic circulation flows down the salinity-induced pressure gradient (up the temperature gradient) across the ice edge, transporting relatively warm open-ocean surface water to under the ice and leading to further melting (Figures 1a and 1d). This melting near the ice edge increases the local salinity gradient, strengthening the jet, which becomes unstable. Eddies grow rapidly at the ice edge (Figures 1a and 1b), exchange salinity laterally and vertically, with strong positive eddy temperature fluxes near the surface under the ice (Figure 1e).

3.1. The Effect of Ocean Circulation on Sea-Ice Melting

Sources of heat that lead to sea-ice melting include surface heating from the atmosphere and heat transport due to the ocean circulation. To separate the two we compare the above results to a similar experiment without an active ocean, in the sense that ocean velocities are set to zero. Given that horizontal diffusion is also zero, only (weak) vertical diffusion occurs in the ocean in this case. Because of the horizontally homogeneous imposed forcing fields, with the ocean inactive, sea ice in each ice-covered grid cell evolves in the same way. Sea-ice volume melt rates are significantly higher with the ocean model active (Figure 2c, black solid line)

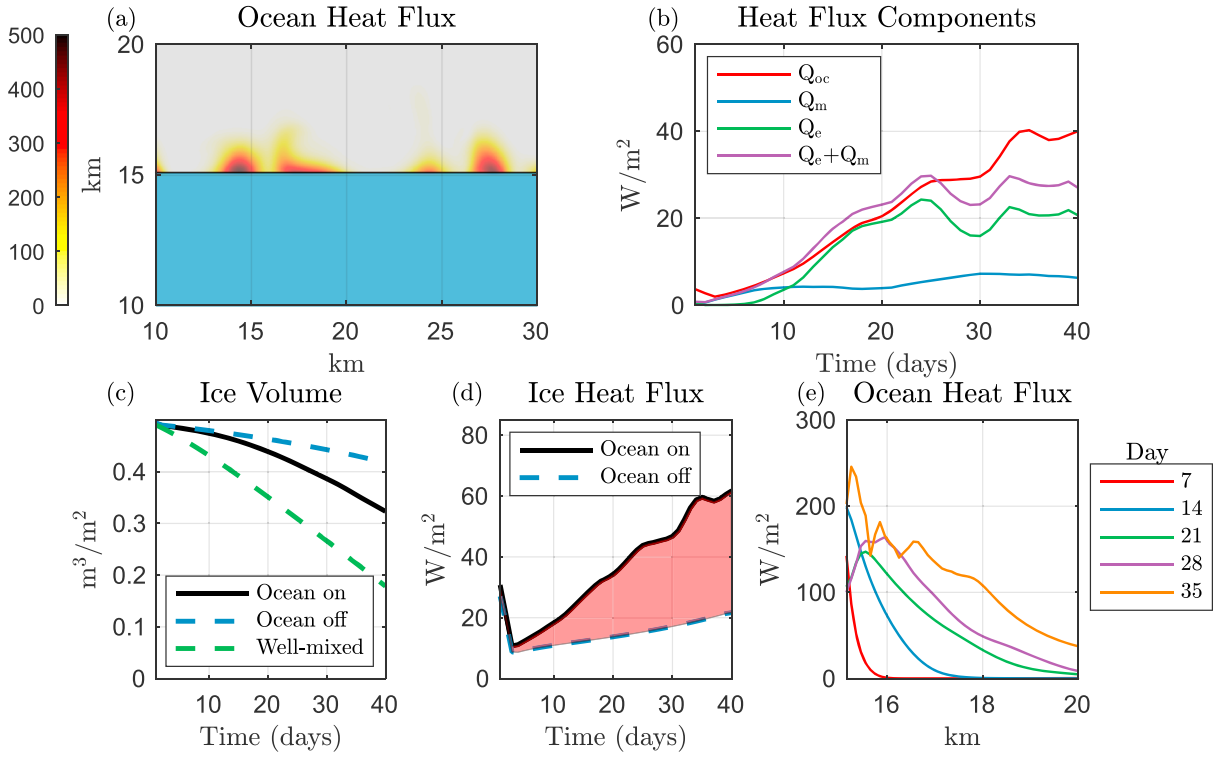

Figure 2. Sea-ice melting and heat fluxes. (a) Heat flux due to ocean circulation, $Q_{oc}(x, t)$, (W/m^2) at model day 14. (b) Domain-averaged heat fluxes from ocean circulation (red line), the zonal-mean circulation (blue line), the effect of ocean eddies (green line), and the sum of the mean and eddy fluxes (purple). (c) Curves of average sea-ice volume as a function of time for (black) the simulation with active ocean, (blue dashed) a simulation with the ocean model inactive, and if the surface ocean heat flux were evenly mixed across the domain (green dashed). (d) Latent heat fluxes derived from sea-ice volume evolution. Red shaded area is the average ocean circulation heat flux $\overline{Q}_{oc}$. (e) Zonal-mean ocean-ice heat flux $\overline{Q}^{x}_{oc}(y, t)$ as a function of cross-channel distance at every 7 days.

compared to when the ocean model is inactive (Figure 2c, blue dashed line), indicating the critical role of heat transport by ocean eddies in leading ice melting. In Figure 2c (green line), we plot the evolution of sea-ice volume, if the ocean surface heating were evenly applied throughout the domain, assuming rapid horizontal mixing within the grid cell, as is currently done in ocean/sea-ice models. A large fraction of this heat flux is absorbed away from the ice, and under the unrealistic assumption of rapid horizontal mixing, sea-ice volume declines significantly more rapidly. For both simulations (active and inactive ocean), we compute a latent heat flux field, $Q(\mathbf{x}, t)$, implied by sea-ice volume changes,

$$Q(\mathbf{x}, t) = L_f \rho_i \frac{\partial V(\mathbf{x}, t)}{\partial t}, \tag{1}$$

where $V(\mathbf{x}, t)$ is the sea-ice volume field. We compute the heat flux due to ocean circulation, $Q_{oc}(\mathbf{x})$, as the difference between the results of the runs with ocean dynamics on and off,

$$Q_{oc}(x, t) = Q_{on}(x, t) - Q_{off}(x, t). \tag{2}$$

We plot the spatial average of each latent heat flux field, $\overline{Q}^{xy}_{on}(t)$ (Figure 2d, black line), $\overline{Q}^{xy}_{off}(t)$ (Figure 2d, blue line), and $\overline{Q}^{xy}_{oc}(t)$ (Figure 2d, red shaded region), where $\overline{(\cdot)}^{xy}$ denotes a horizontal average. $\overline{Q}^{xy}_{oc}$ grows to 21 W/m^2 after 21 days, significantly larger than the "ocean off" heat flux of 14 W/m^2 at the same time. By day 40, $\overline{Q}^{xy}_{oc}$ is 40 W/m^2 compared to $\overline{Q}^{xy}_{off}$ = 21 W/m^2. Figure 2a shows $Q_{oc}(x, t)$ at day 14, with the along-ice-edge mean $\overline{Q}^{x}_{oc}(y, t)$ plotted in Figure 2e every 7 days, showing how the heat flux due to ocean dynamics spreads under the ice as the eddies strengthen.

Local values of $Q_{oc}(x, t)$ can exceed several hundred W/m^2 when the ocean is actively transporting warm water underneath the ice (warm colors, Figure 2a). This demonstrates the critical role of ocean dynamics due to eddy mixing in melting floes near the edges, a process not represented in current climate models, and therefore

requiring a parameterization. Under the ice, and far from the ice edge, $Q_{oc}(x,t) \approx 0$, in contradiction to the assumption of instantaneous mixing employed in current GCMs.

3.2. The Effect of Eddies on Sea-Ice Melting

The time evolution of the zonal-mean ocean temperature is

$$\frac{\partial \overline{T}^x}{\partial t} + \overline{\mathbf{u}}^x \cdot \nabla \overline{T}^x = \overline{S}^x[T] - \nabla \cdot (\overline{u'T'}^x, \overline{v'T'}^x, \overline{w'T'}^x) = \overline{S}^x[T] - \nabla \cdot \mathbf{F}[T], \tag{3}$$

where primed quantities are anomalies from the zonal mean, $\mathrm{u} = (u, v, w)$ is the ocean velocity field, T the temperature, $S[T]$ is the surface source of buoyancy including heat fluxes and sea-ice melting, and $\mathbf{F}[C]$ denotes the zonal mean flux of the tracer C by the eddy field.

We integrate equation (3) in ice-covered regions over a depth H, and multiply by the ocean specific heat capacity, c_p, and density, ρ_0, leading to the zonal-mean heat budget of this surface layer,

$$\begin{aligned} & c_p \rho_0 \int_{-H}^{0} dz \frac{\partial \overline{T}^x}{\partial t} \\ & = Q_s - L_f \rho_i \frac{\partial \overline{V}^x}{\partial t} - c_p \rho_0 \int_{-H}^{0} dz \left(\overline{\mathbf{u}}^x \cdot \nabla \overline{T}^x - \nabla \cdot \mathbf{F} \right) \\ & = Q_s - L_f \rho_i \frac{\partial \overline{V}^x}{\partial t} + Q_m + Q_e, \end{aligned} \tag{4}$$

where Q_s is the net surface heating by air-sea fluxes, Q_m is the heating by zonal mean ocean flows, and Q_e is the eddy heat flux. Under the ice, we assume the ocean temperature is approximately at freezing, and therefore $\partial \overline{T}^x / \partial t \equiv 0$, such that the left-hand side of the above equation vanishes. Averaging each term over the entire ice-covered domain, we obtain an equation for the evolution of sea-ice volume,

$$L_f \rho_i \frac{\partial V}{\partial t} = Q_{on/off} = Q_m + Q_e + Q_s. \tag{5}$$

With the ocean circulation off, $Q_m = Q_e = 0$, and,

$$Q_{oc} \equiv Q_{on} - Q_{off} \approx Q_m + Q_e \tag{6}$$

In general, the under-ice temperature is slightly above freezing as the heat transported to under the ice floe is not instantaneously absorbed by the ice base, though approximating the temperature to be at freezing under the ice is appropriate throughout the experiment period shown in Figure 2.

Figure 2b plots the terms in (6), the area-averaged contributions to the total sea-ice melting due to ocean dynamics, Q_{oc} (red, also shown by the shaded region in Figure 2d). The melting heat flux due to the mean ocean currents grows (blue) and saturates at about 4 W/m^2 by day 7. The heat flux due to eddies (green) grows rapidly, surpassing Q_m by day 12, increasing by roughly 1.5 W/m^2 per day, reaching 20 W/m^2 by day 20. Over this period, the sum of ocean heat fluxes computed via equation (6) (Figure 2b, purple) tracks Q_{oc}, justifying our previous assumptions. Over time, as the sea-ice edge begins to depart from zonal symmetry, the approximations used to derive equation (6) are no longer valid.

3.3. Parameterizing Sea-Ice Melting due to Ocean Eddies

In current climate models, subgrid-scale sea-ice floes and ocean eddies are not resolved, and heat absorbed by an open ocean area is immediately distributed under the ice within the same grid box, as demonstrated above. Because the effect of eddies leads to a significant difference in ice evolution both from this well-mixed assumption and from the assumption of no ocean dynamics (Figure 2c) we wish to correctly represent the eddy heat transport between ice-covered and ice-free regions, and the resulting contribution to ice melting, Q_{oc} (equation (6)). We seek a simple parameterization of the eddy heat exchange that we showed above to control sea-ice melting.

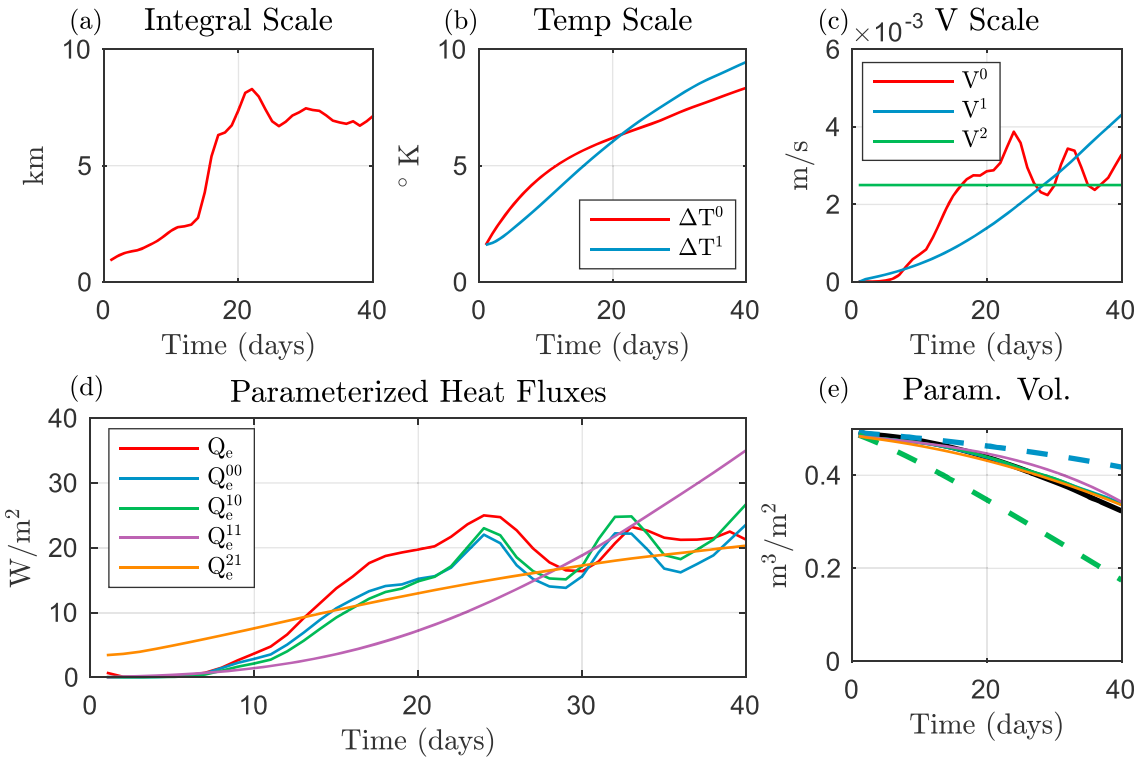

Figure 3. Components of, and parameterization of, the eddy heat flux Q_e. (a) The eddy length scale ΔX computed from model results. (b) The two-box temperature difference between ice and ice-free regions, computed from the modeled ocean temperature fields (red) or computed from balancing the ocean surface warming with latent heat from sea-ice melting (blue). (c) Velocity scaling estimates for the cross-ice velocity V using the quasigeostrophic scaling of Andrews and McIntyre (1978), either computed directly (red), based on the scaling of Haine and Marshall (1998) (blue), or a constant estimate (green). (d) Estimates of the eddy heat flux compared to its computed value (red). Definitions of each estimate of Q_e are tabulated in Table 1. Using computed values of ΔT and V ($Q_e^{(0,0)}$, blue), an estimate of ΔT with V computed from model results ($Q^{(1,0)}$, green), an estimate of ΔT with parameterized V from Haine and Marshall (1998) ($Q_e^{(1,1)}$, purple), or an estimate of ΔT with a fixed V ($Q_e^{(1,2)}$, orange) (e) Same as Figure 2c, including volume curves obtained by integrating equation (5) with $Q_m = 4\text{W/m}^2$ and Q_e defined by the parameterizations in (d).

Consider the heat budget of two regions: one corresponding to the top H meters of the ice-free region and the other to the top H meters of the ice-covered region. The ice-free regions are characterized by a freely varying temperature, T_o, and salinity, S_o, and the under-ice regions have a variable salinity, S_i, with temperature assumed fixed at the ocean freezing point, T_f.

While the secondary circulation develops faster than the eddies, its effect on melting is significantly smaller than that of eddies once they reach finite amplitude. We estimate Q_e according to the following scaling,

$$Q_e \approx c_p \rho V \frac{\Delta T}{\Delta X}, \tag{7}$$

with units of W/m^2. The factor $\Delta T = T_o - T_f$ is the temperature difference between the ice-free and ice-covered regions, ΔX is the eddy length scale, and the velocity V represents the strength of the eddy exchange. The length scale ΔX is calculated as the decorrelation length scale of the meridional velocity field, estimated as the distance corresponding to the first zero of the correlation function $C(y,\xi) = \overline{v(x,y)v(x+\xi,y)}^{x}$. The time evolution of ΔX is shown in Figure 3a, and based on this as well as for simplicity, we fix $\Delta X = 5$ km in all cases, assuming the effect of eddies is felt roughly 2.5 km into the ice edge.

We now develop a sequence of approximations for the eddy heat flux contribution to the sea-ice melting, Q_e, summarized in Table 1, culminating with a version that can serve as the base for a parameterization in future climate models. We begin by approximating the melting effect of ocean eddies using the full model output. The red line in Figure 3b shows ΔT^0, computed as the difference in temperature between the ice-covered and ice-free regions over a depth $H = 5$ m. To estimate the eddy velocity, we use a quasigeostrophic scaling (Andrews & McIntyre, 1978), for the eddy-induced overturning velocity,

Table 1
Definitions of the Ocean Eddy Heat Flux Q_e and Parameterizations Detailed in the Text, Along with their Depiction in Figure 3d

Name	Estimate of Δ T	Estimate of V	Color in Figure 3d
Q_e	— Computed via equation (6) —		Red
$Q_e^{(0,0)}$	From Simulation	From Simulation (equation (8))	Blue
$Q_e^{(1,0)}$	Equation (9)	From Simulation (equation (8))	Green
$Q_e^{(1,1)}$	Equation (9)	Equation (13)	Purple
$Q_e^{(1,2)}$	Equation (9)	Constant	Orange

Note. Estimates of *T* and *V* form the components of equation (7). The superscript indices on *Q* refer to the level of approximation used for the cross ice-edge temperature difference and for the velocity scale, correspondingly.

$$v \approx \frac{\partial}{\partial z}\left(\overline{v'b'}/\bar{b}_z\right). \tag{8}$$

The first estimate of the eddy velocity scale, V^0, is computed as the average of v over a depth H at the ice edge (Figure 3c, red).

The first estimate for the eddy-induced melting heat flux, computed directly from the simulation output fields, is denoted $Q_e^{(0,0)}$ (Figure 3d, blue), and completes equation (7) using V^0 and T^0. A list of all notation and variants of the parameterization presented is given in Table 1, along with their colors in Figure 3d. The approximation $Q_e^{(0,0)}$ is well-correlated with the eddy contribution to the melting heat flux, Q_e (Figure 3d, red) over the first 40 days, with a correlation coefficient $r^2 = 0.81$ between the two detrended time series, which in addition to the visual confirmation of Figure 3d gives confidence that the downgradient approximation of equation (7) can estimate the melting rate of sea ice in this context.

Climate models may not resolve the required horizontal variation in temperature or circulation, and therefore we seek alternative representations of V and T based on properties of the large-scale forcing. The time rate of change of the ice-free surface temperature is a function of the surface heat flux over open water, Q_s, with units W/m^2 of open water. The average of this flux over the entire model domain (or over a grid cell of a global climate model) is equal to ϕQ_s, where ϕ is the open water fraction. Neglecting vertical mixing of heat, the remaining sink of surface heat is latent heat used to melt sea ice after being transported across the ice edge (the ice-covered surface ocean region is assumed to stay at its freezing point). We approximate,

$$Hc_p\rho\phi\frac{\partial T_o}{\partial t} \approx Q_s\phi - Q_e, \tag{9}$$

We choose $H = 5$ m based on the resolved density profile of the ice-free ocean (i.e., Figure 1f), which evolves as a function of depth due to the exponential penetration of shortwave radiation and the growing ocean circulation. As the left-hand side of equation (9) represents the heat content available to melt sea ice, choosing a larger value of H incorporates subsurface waters separated from the surface warming and ice base that do not lead to melting. We repeat Figures 3d and 3e using $H = 10$ in Figures S3a and S3c. In that case Q_e is underestimated.

Figure 3b shows the parameterized $\Delta T^1 = T_o - T_f$ (blue line) calculated using (9). This approximation underestimates the warming of the surface layer initially, and overestimates it at later times but is adequate overall. An estimate of the eddy heat flux using ΔT^1 and V^0, $Q_e^{1,0}$, (Figure 3d, green) is well correlated with the computed eddy heat flux Q_e over this period (detrended $r^2 = 0.66$)

Next, in equation (10), we scale the magnitude of the meridional eddy flux according to Haine and Marshall (1998), with $\overline{v'b'}^x \approx -C_1\bar{b}_z H^2\overline{b}_y^x/f$, where C_1 is a nondimensional "efficiency parameter,"

$$v \sim \frac{\partial}{\partial z}\left(\frac{\overline{v'b'}^x}{\overline{b}_z^x}\right) \approx \frac{1}{H}\left(\frac{\overline{v'b'}^x}{\overline{b}_z^x}\right) \approx -C_1\frac{H}{f}\overline{b}_y^x \approx C_1\frac{-H}{f}\frac{\Delta B}{\Delta X} \tag{10}$$

We approximate the change in buoyancy resulting from salinity variations alone using a linear equation of state, $\rho = \rho_0(1 + \beta(S - S_0))$. We express the buoyancy difference between ice-free and ice-covered regions as,

$$\Delta B = -g\beta\Delta S, \tag{11}$$

where $\beta \approx 8{\cdot}10^{-4}$ psu^{-1}. The time rate of change of the salt content of the upper layer of the under-ice regions is equal to $c\rho_0 H\partial S_i/\partial t$, where $c = 1 - \phi$ is the sea-ice concentration and S_i is the under-ice salinity. Assuming the sea ice to be fresh, the freshwater flux due to melting sea ice is $\rho_i \partial V_i/\partial t$ kg m^{-2} s^{-1}, and therefore the time rate of change of the under-ice salinity is expressed in terms of the melting of sea ice,

$$\frac{\partial S_i}{\partial t} = -\frac{S_i}{H}\frac{\rho_i}{\rho_0}\frac{\partial V_i}{\partial t}\frac{1}{c}. \tag{12}$$

We now estimate the eddy velocity scale by integrating the under-ice salinity equation, finding,

$$V^1 = C_1\frac{g\beta}{f\Delta X}\frac{\rho_i}{\rho_0}\int S_i\frac{\partial V_i}{\partial t}\frac{1}{c}dt. \tag{13}$$

Importantly, all quantities in equation (13) can be computed in a coarse climate model. We find $C_1 \approx 0.1$ gives the best fit to Q_e, and plot $V^{(1)}$ as a blue line in Figure 3c. The estimate $Q_e^{1,1}$ is computed from ΔT^1 and $V^{(1)}$ (Figure 3d, purple line) and, even with the broad simplification of equation (13), represents the general trend in Q_e. This parameterization may be evaluated in a climate model, by integrating forward equations starting from the time at which the net heat flux is generally warming, and sea ice begins to melt. In practice, to correctly estimate the mixing of ice-free and ice-covered regions would require tracking the ice-free surface temperature, under-ice surface temperature, and under-ice salinity separately (using a scheme like that designed by Holland, 2003, or Roach et al., 2018).

We compute a simpler estimate for the contribution of subgrid-scale ocean eddies to sea ice, fixing the cross-ice velocity scale $V^{(2)} = 2$ mm/s (green line, Figure 3c) and thereby dropping the need to track under-ice salinity. The resulting estimate for the eddy heat flux, $Q_e^{(1,2)}$ (orange line, Figure 3d) represents the trend in Q_e but over-estimates the rate of sea-ice melting when the eddies are inactive. Figure 3e superimposes on top of Figure 2c curves of sea-ice volume obtained by integrating forward equation 5 using $Q_m \equiv 4$ W/m^2 and for each of the parametrizations of Q_e plotted in Figure 3e. Each parameterized volume curve approximates the resolved volume curve better than the assumption of no mixing or perfect horizontal mixing.

In Figures S1–S3, we test the robustness of the results by plotting the same diagnostics in Figure 3d and 3e, altering the initial applied heat forcing, shrinking the mixed layer from 50 m, allowing the stratification to reach closer to the surface, and changing the ice-ocean heat transfer coefficient by a factor of ± 2. Generally, the parameterization is robust to these significant changes. The parameterization is not effective for the largest external forcings (an initial net heating of 130 W/m^2 and above): In this case there are earlier deviations from from the assumptions made in equation (6), such as a departure from zonal symmetry and strong surface melting of the ice. When we reduce the initial mixed layer depth to 10 m and below, the instability is suppressed, and $Q_e \approx 0$. In these shallow cases there is significant partitioning or heat between ice and ocean, and even erroneously large eddy mixing effects provide a better estimate of the sea-ice volume curve than the well-mixed assumption (Figure S1d).

4. Discussion and Conclusions

Using simulations of an ocean near a sea-ice edge in a domain corresponding to a single climate model grid cell, we developed and examined a scaling argument describing the effects on melting due to eddies generated at the edge of a floe that can be used in future climate models. The scaling derived here reproduces the modeled sea-ice volume evolution over a period of 40 days, corresponding to a significant portion of the sea-ice melting season, as a function of model state variables that are resolved by coarse-grid sea ice and climate models.

The study of emergent subgrid-scale sea-ice state variables such as the floe size distribution and their effect on large-scale climate is growing rapidly (e.g., Bennetts et al., 2017; Horvat & Tziperman, 2015, 2017; Roach et al., 2018; Zhang et al., 2016). More work is needed to investigate how the results obtained here can be applied to generalized floe geometry and to constrain the relative strength of the effect of eddies versus other processes that mix heat in the upper ocean, including wind, waves, and sea-ice motion. In order for the work presented here to be used to improve upon the currently used implicit instantaneous numerical "mixing" of

heat between open ocean and sea ice within a given grid cell, a full assessment will be needed of the mixing processes that transfer heat in the upper ice-covered oceans.

The scenario examined in this paper does not include sea ice forced by large-scale wind or ocean currents, though drift speeds of sea-ice floes can be up to 10 km/day (Kwok et al., 2013). Instability growth rates examined here are O(1/day), and eddy scales of O(2 km), suggesting the analysis presented above is appropriate only in situations where ice drift speeds are O(1 km/day) and lower. To modify the parameterization above for such dynamical scenarios would likely require experiments with moving, thermodynamically active sea-ice floes that resolve both the sharp gradients in surface forcing at the edge of floes but also their drift forced by wind and ocean current. The instability investigated here competes with and is modified by other effects, and represents but one of several mixing processes that can influence the sea ice. For example, stresses from ice or ocean motions can lead to shear that will enhance vertical mixing and energize an Ekman overturning circulation, both of which will deepen the freshwater lens that forms under the melting ice and may lead to dynamical instabilities (Hakkinen, 1986; Manucharyan & Thompson, 2017).

Describing the rich interactions between eddies and sea-ice melting, including the many processes merely briefly discussed above, remains an open and important problem, yet there have to date been no observational investigations of the melting of a single floe nor the developing ocean circulation at the floe edge. Field observations will be an important part of constraining these processes, and together with floe-scale process modeling, will lead to a better representation of the effects of small-scale ice-ocean interactions on high-latitude climate.

Acknowledgments
The authors would like to thank Andy Hogg and two anonymous reviewers for their most constructive comments. Files required to reproduce experiments shown here are publicly available at http://web-static-aws.seas.harvard.edu/climate/eli/Downloads/. This work was funded by NSF Physical Oceanography program, grant OCE-1535800 and by the NASA ROSES program, grant NNX14AH39G. C. H. was supported by the NOAA Climate and Global Change Postdoctoral Fellowship Program, administered by UCAR's Cooperative Programs for the Advancement of Earth System Science (CPAESS), sponsored in part through cooperative agreement NA16NWS4620043, Years 2017–2021, with the National Oceanic and Atmospheric Administration (NOAA), U.S. Department of Commerce (DOC). The views expressed in this paper are those of the author(s) and do not necessarily reflect the view of DOC, any of its subagencies, or any other Sponsors of CPAESS and/or UCAR. E. T. thanks the Weizmann Institute for its hospitality during parts of this work. C. H. thanks the National Institute of Water and Atmospheric Science as well as the Frenchboro Trust for their hospitality during parts of this work.

References

Andrews, D. G., & McIntyre, M. E. (1978). Generalized Eliassen-palm and Charney-drazin theorems for waves oin axismmetric mean flows in compressible atmospheres. *Journal of the Atmospheric Sciences*, *35*(2), 175–185. https://doi.org/10.1175/1520-0469(1978)035<0175:GEPACD>2.0.CO;2

Årthun, M., Holland, P. R., Nicholls, K. W., & Feltham, D. L. (2013). Eddy-driven exchange between the open ocean and a subice shelf cavity. *Journal of Physical Oceanography*, *43*(11), 2372–2387. https://doi.org/10.1175/JPO-D-13-0137.1

Bennetts, L. G., O'Farrell, S., & Uotila, P. (2017). Brief communication: Impacts of ocean-wave-induced breakup of Antarctic sea ice via thermodynamics in a stand-alone version of the CICE sea-ice model, *11*(3), 1035–1040. https://doi.org/10.5194/tc-11-1035-2017

Carton, J. A., & Giese, B. S. (2008). A reanalysis of ocean climate using simple ocean data assimilation (SODA). *Monthly Weather Review*, *136*(8), 2999–3017. https://doi.org/10.1175/2007MWR1978.1

Deremble, B., Wienders, N., & Dewar, W. K. (2013). CheapAML: A simple, atmospheric boundary layer model for use in ocean-only model calculations. *Monthly Weather Review*, *141*(2), 809–821. https://doi.org/10.1175/MWR-D-11-00254.1

Haine, T. W. N., & Marshall, J. (1998). Gravitational, symmetric, and baroclinic instability of the ocean mixed layer. *Journal of Physical Oceanography*, *28*(4), 634–658. https://doi.org/10.1175/1520-0485(1998)028<0634:GSABIO>2.0.CO;2

Hakkinen, S. (1986). Coupled ice-ocean dynamics in the marginal ice zones: Upwelling/downwelling and eddy generation. *Journal of Geophysical Research*, *91*(C1), 819–832. https://doi.org/10.1029/JC091iC01p00819

Holland, M. M. (2003). An improved single-column model representation of ocean mixing associated with summertime leads: Results from a SHEBA case study. *Journal of Geophysical Research*, *108*(C4), 3107. https://doi.org/10.1029/2002JC001557

Horvat, C., & Tziperman, E. (2015). A prognostic model of the sea-ice floe size and thickness distribution. *Cryosphere*, *9*(6), 2119–2134. https://doi.org/10.5194/tc-9-2119-2015

Horvat, C., & Tziperman, E. (2017). The evolution of scaling laws in the sea ice floe size distribution. *Journal of Geophysical Research: Oceans*, *122*, 7630–7650. https://doi.org/10.1002/2016JC012573

Horvat, C., Tziperman, E., & Campin, J. M. (2016). Interaction of sea ice floe size, ocean eddies, and sea ice melting. *Geophysical Research Letters*, *43*, 8083–8090. https://doi.org/10.1002/2016GL069742

Kwok, R., & Rothrock, D. A. (2009). Decline in Arctic sea ice thickness from submarine and ICESat records: 1958-2008. *Geophysical Research Letters*, *36*, L15501. https://doi.org/10.1029/2009GL039035

Kwok, R., Spreen, G., & Pang, S. (2013). Arctic sea ice circulation and drift speed: Decadal trends and ocean currents. *Journal of Geophysical Research: Oceans*, *118*, 2408–2425. https://doi.org/10.1002/jgrc.20191

Large, W. G., McWilliams, J. C., & Doney, S. C. (1994). Oceanic vertical mixing: A review and a model with a nonlocal boundary layer parameterization. *Reviews of Geophysics*, *32*(4), 363–403. https://doi.org/10.1029/94RG01872

Lei, R., Li, N., Heil, P., Cheng, B., Zhang, Z., & Sun, B. (2014). Multiyear sea ice thermal regimes and oceanic heat flux derived from an ice mass balance buoy in the Arctic Ocean. *Journal of Geophysical Research: Oceans*, *119*, 537–547. https://doi.org/10.1002/2012JC008731

Losch, M., Menemenlis, D., Campin, J. M., Heimbach, P., & Hill, C. (2010). On the formulation of sea-ice models. Part 1: Effects of different solver implementations and parameterizations. *Ocean Modelling*, *33*(1-2), 129–144. https://doi.org/10.1016/j.ocemod.2009.12.008

Manucharyan, G. E., & Thompson, A. F. (2017). Submesoscale sea ice-ocean interactions in marginal ice zones. *Journal of Geophysical Research Ocean*, *122*, 9455–9475. https://doi.org/10.1002/2017JC012895

Markus, T., Stroeve, J. C., & Miller, J. (2009). Recent changes in Arctic sea ice melt onset, freezeup, and melt season length. *Journal of Geophysical Research*, *114*, C12024. https://doi.org/10.1029/2009JC005436

Marshall, J., Hill, C., Parelman, L., & Adcroft, A. (1997). Hydrostatic, quasy-hydrostatic, and non-hydrostatic ocean modeling. *Journal of Geophysical Research*, *102*(C3), 5733–5752.

Maslanik, J., Stroeve, J., Fowler, C., & Emery, W. (2011). Distribution and trends in Arctic sea ice age through spring 2011. *Geophysical Research Letter*, *38*, L13502. https://doi.org/10.1029/2011GL047735

Matsumura, Y., & Hasumi, H. (2008). Brine-driven eddies under sea ice leads and their impact on the Arctic Ocean mixed layer. *Journal of Physical Oceanography*, *38*(1), 146–163. https://doi.org/10.1175/2007JPO3620.1

McPhee, M. G. (1992). Turbulent heat flux in the upper ocean under sea ice. *Journal of Geophysical Research*, *97*(C4), 5365–5379. https://doi.org/10.1029/92JC00239

McPhee, M. G., & Morison, J. H. (2008). *Under-Ice Boundary Layer*, *Encycl. Ocean Sci.* (2nd ed., pp. 155–162). New York: Elsevier. https://doi.org/10.1016/B978-012374473-9.00146-6

Peralta-Ferriz, C., & Woodgate, R. A. (2015). Seasonal and interannual variability of pan-Arctic surface mixed layer properties from 1979 to 2012 from hydrographic data, and the dominance of stratification for multiyear mixed layer depth shoaling. *Progress in Oceanography*, *134*, 19–53. https://doi.org/10.1016/j.pocean.2014.12.005

Perovich, D. K. (2003). Thin and thinner: Sea ice mass balance measurements during SHEBA. *Journal of Geophysical Research*, *108*(C3), 8050. https://doi.org/10.1029/2001JC001079

Roach, L. A., Horvat, C., Dean, S. M., & Bitz, C. M. (2018). An emergent sea ice floe size distribution in a global coupled ocean-sea ice model. *Journal of Geophysical Research: Oceans*, *123*, 4322–4337. https://doi.org/10.1029/2017JC013692

Screen, J. A., & Simmonds, I. (2010). The central role of diminishing sea ice in recent Arctic temperature amplification. *Nature*, *464*(7293), 1334–1337. https://doi.org/10.1038/nature09051

Steele, M. (1992). Sea ice melting and floe geometry in a simple ice-ocean model. *Journal of Geophysical Research*, *97*(C11), 17,729–17,738. https://doi.org/10.1029/92JC01755

Stroeve, J. C., Serreze, M. C., Holland, M. M., Kay, J. E., Malanik, J., & Barrett, A. P. (2012). The Arctic's rapidly shrinking sea ice cover: A research synthesis. *Climate Change*, *110*(3-4), 1005–1027. https://doi.org/10.1007/s10584-011-0101-1

Winton, M. (2000). A reformulated three-layer sea ice model. *Journal of Atmospheric and Oceanic Technology*, *17*(4), 525–531. https://doi.org/10.1175/1520-0426(2000)017<0525:ARTLSI>2.0.CO;2

Zhang, J., Stern, H., Hwang, B., Schweiger, A., Steele, M., Stark, M., & Graber, H. C. (2016). Modeling the seasonal evolution of the Arctic sea ice floe size distribution. *Elementa: Science of the Anthropocene (Washington, DC)*, *4*(1), 000126. https://doi.org/10.12952/journal.elementa.000126